Catalytic decomposition of ethanol on $V_2O_5/AlPO_4$ catalysts

Abd El-Aziz A Said[1]* and Kamal MS Khalil[2]
[1]Chemistry Department, Faculty of Science, Assiut University, Assiut, Egypt
[2]Chemistry Department, Faculty of Science, South Valley University Sohag, Egypt

Abstract: Different ratios of vanadium pentoxide supported on aluminum phosphate (1–30 mol%) have been prepared by an impregnation method. The original and calcined samples were characterized by TG, DTG, DSC, X-ray diffraction, IR spectra, N_2 adsorption and electrical conductivity measurements. The catalytic decomposition of ethanol has been carried out at 210 °C in a flow system at 1 atm using air as a carrier gas. The results indicate that the catalysts calcined at 400 °C were active and selective towards ethene formation whereas the samples calcined at 600 °C showed a drastic reduction in both activity and selectivity.

Keywords: vanadium pentoxide; aluminum phosphate; supported catalysts; decomposition of ethanol

1 INTRODUCTION

The catalytic activity and selectivity of metal oxide catalysts may be greatly influenced by the type of support. Aluminum phosphate ($AlPO_4$), a material with good thermal stability and large pores belongs to a family of recently developed high-surface area aluminophosphate supports. This group of materials has received increasing attention and intensive study as potential supports for polymerization, for hydrogenation reactions and as partial oxidation catalysts.[1–4] Vanadium oxide catalysts in combination with various supports are well known for catalyzing a great variety of reactions including partial oxidation and amoxidation of various hydrocarbons.[5–8] Therefore, it is common to support (to disperse and stabilize) the active vanadia phase on Al_2O_3, SiO_2, MgO or TiO_2. However, in many experimental studies, the limitations of the currently available bulk and surface characterization techniques have been coupled with the complex solid–solid interaction between V_2O_5 and $AlPO_4$ to detect the different types of active phase. Moreover, various vanadium phosphates have been detected in the VPO catalysts, depending on the methods of preparation and conditioning of the conventional catalyst precursor. The current literature demonstrates the lack of agreement on the nature of the active phase.[9–11] In addition, one of the most important problems of the supported metal oxide catalysts is the establishment of a close relationship between the catalytic activity and the physicochemical properties of the active phase. Therefore, the connection between the catalytic activity of the V_2O_5 and $AlPO_4$ system and its structure needs further study. The present work relates the influence of the catalyst structure, which forms as a result of the interaction between V_2O_5 and $AlPO_4$, to the catalytic conversion of ethanol.

2 EXPERIMENTAL

2.1 Materials

The starting materials $AlPO_4$ (AP) (Merck) and NH_4VO_3 (AMV) (BDH) were used in preparation of the catalysts without modification. The mixed samples were prepared by impregnation of $AlPO_4$ with different proportions of ammonium metavanadate dissolved in doubly-distilled water. Yellow mixtures were formed which denoted the formation of a new phase.[12] The samples produced were dried in an oven at 100 °C for 24 h before being calcined at 400 °C and 600 °C for 4 h in static air. The content of V_2O_5 was 1, 3, 5, 7, 10, 15, 20 and 30 mol%. Analytical grade ethanol (BDH Ltd) was refluxed with sodium and distilled before use in catalytic runs. Its purity was checked by GC.

2.2 Apparatus and techniques

2.2.1 *Thermal analyses*

A thermal analyzer 2000 TA instrument (USA) controlling a 2050 thermogravimetric (TG) analyzer and 2010 differential scanning calorimeter (DSC) was used. For TG a ceramic sample boat was used with the sample size being 10.0 ± 0.1 mg. Curves were recorded upon heating up to 600 °C at 10 °C min^{-1} and a 30 cm^3 min^{-1} flow of a nitrogen atmosphere. For DSC measurements, a sample size of 5.0 ± 0.1 mg was

* Correspondence to: Abd El-Aziz A Said, Chemistry Department, Faculty of Science, Assiut University, Assiut, Egypt
E-mail: Assiut@Frcu.eun.eg
(Received 4 January 1999; revised version received 2 September 1999; accepted 22 October 1999)

heated up to 500 °C in a covered aluminum sample pan at 10 °C min^{-1} and a flow of 30 cm^3 min^{-1} of nitrogen gas.

2.2.2 X-ray diffractometry

XRD of the test samples was performed with a Philips diffractometer (Model PW 2103, 35 kV and 20 mA) with a source of CuK_α radiation (Ni-filtered). The diffraction lines of the characterized samples were matched with ASTM cards.[13]

2.2.3 Nitrogen gas adsorption

Nitrogen gas adsorption/desorption isotherms were measured at −196 °C using a model ASAP 2010 instrument (Micromeritics Instrument Corporation, USA). Test samples were thoroughly outgassed for 2 h at 200 °C. The specific surface area, S_{BET}, was calculated applying the BET equation [R1]. Pore volume distribution curves were generated by BET plus V1.00 (2010) software for the instrument indicated, implementing the original density function theory, and slit pores shape [R2].

2.2.4 IR spectroscopy

IR spectra of the original samples and those calcined at 400 °C and 600 °C for 4 h were recorded in the 4000–400 cm^{-1} region with a Shimadzu spectrophotometer model 740 using the KBr disc technique.

2.2.5 Electrical conductivity

The electrical conductivity measurements were carried out using a conductivity cell described previously.[14]

2.2.6 Catalytic activity

Catalytic conversion of ethanol was carried out in a conventional fixed-bed flow type reactor. The system comprised two reactors, one of them was used without any catalyst (control reactor), which enabled a measurement of the blank conversion which was substracted from that measured with the flow reactor. The exit feed was analyzed by direct sampling of the gaseous products into a Unicam gas chromatograph. Thus, the amount of ethanol and its decomposition products was determined. All the measurements were made after steady-state conditions had been reached.

3 RESULTS AND DISCUSSION

3.1 Thermogravimetric analysis

TG and DTG curves of pure AP and mixed with AMV are shown in Figs 1 and 2. The TG analysis of pure AP (curve a) shows that AP loses weight with heating over two stages. The first step that becomes evident is at 100 °C where a weight loss (11%) corresponding to the desorption of physisorbed water is observed. The second step, the major weight loss of 17.3% occurs at 100–400 °C and is due to the loss of strongly adsorbed water and other volatile compounds. Pure AMV (curve h) exhibits weight loss on heating in three steps which are evident at 197, 225 and 320 °C. The first stage which is followed by an 11.7% loss in weight,

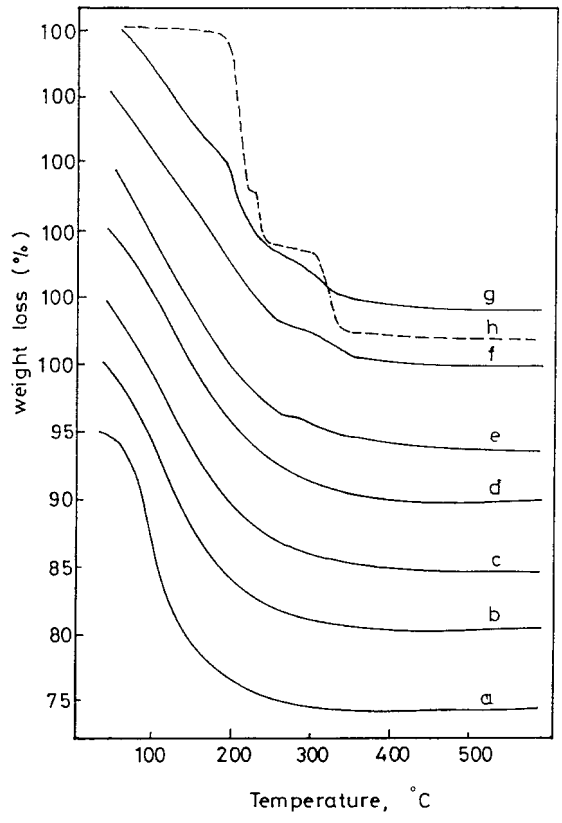

Figure 1. TG curves of pure AP (a) and AMV supported on AP: 3% (b); 7% (c); 10% (d); 15% (e); 20% (f); 30% (g); and pure AMV (h).

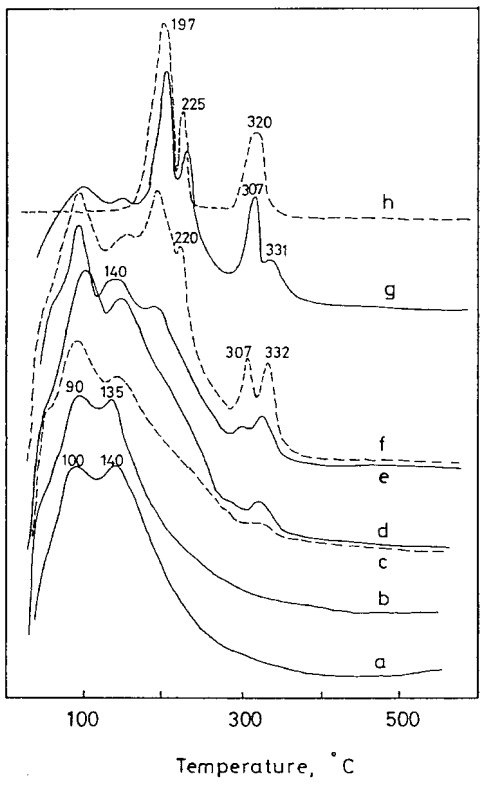

Figure 2. DTG curves of pure AP (a) and AMV supported on AP: 3% (b); 7% (c); 10% (d); 15% (e); 20% (f); 30% (g); and pure AMV (h).

indicates the decomposition of AMV to intermediate ammonium bivanadate (ABV). The second stage accompanied by a loss of 4.2% corresponds to the decomposition of ABV to the intermediate ammonium hexavanadate (AHV). The third stage which was followed by a 6.3% weight loss corresponds to the decomposition of AHV to produce V_2O_5.[15] Curves b–g represent the TG and DTG curves of different ratios of AMV supported on AP. The analysis of the data of the thermal behavior of different solids indicates some trends, and the following conclusions may be drawn.

(i) The weight loss on heating up to 200 °C exhibits two peaks which reach a maximum value at 90 and 140 °C for all samples.
(ii) On addition of 15 mol% AMV, four peaks start to appear at 190, 200, 307 and 330 °C which become sharp and strong on increasing the percentage ratio of AMV up to 30 mol%. These peaks correspond to the decomposition of AMV into V_2O_5. It is important to mention here that no weight loss was observed on increasing the heating temperature up to 600 °C.

Figure 3 shows the DSC results of pure AP and mixed with AMV Curve a shows that AP exhibits one broad endothermic peak which reached a maximum at 130 °C. The endothermic behavior below 200 °C illustrates the well known weight loss due to the removal of crystalline water. On the other hand the pure AMV curve exhibits a sharp and strong endothermic peak located at 243 °C and a small exothermic peak with a maximum at 425 °C. Curves b–g for the supported samples show new endothermic peaks which reached their maximum values at about 330, 350, and 440 °C on addition of 7 mol% AMV. These peaks become stronger and sharper on increasing the content of AMV up to 30 mol%. These new peaks may be attributed to the interaction between V_2O_5 and $AlPO_4$ to produce a new phase, as illustrated by the XRD.

3.2 IR spectra

IR spectra of original and calcined samples of pure AP and mixed with AMV are shown in Figs 4–6. Figures 4 and 5 represent the spectra of original samples and those calcined at 400 °C. These two figures show the following observations.

(i) Pure AP (curve a) shows three absorption bands. The first one, assigned at 3793 cm^{-1} was characteristic of surface Al—OH, the second band, which appeared at 1628 cm^{-1}, was due to the presence of Brønsted acid sites.[16] The third band in the region between 1200 and 1000 cm^{-1} was probably due to the different internal stretching

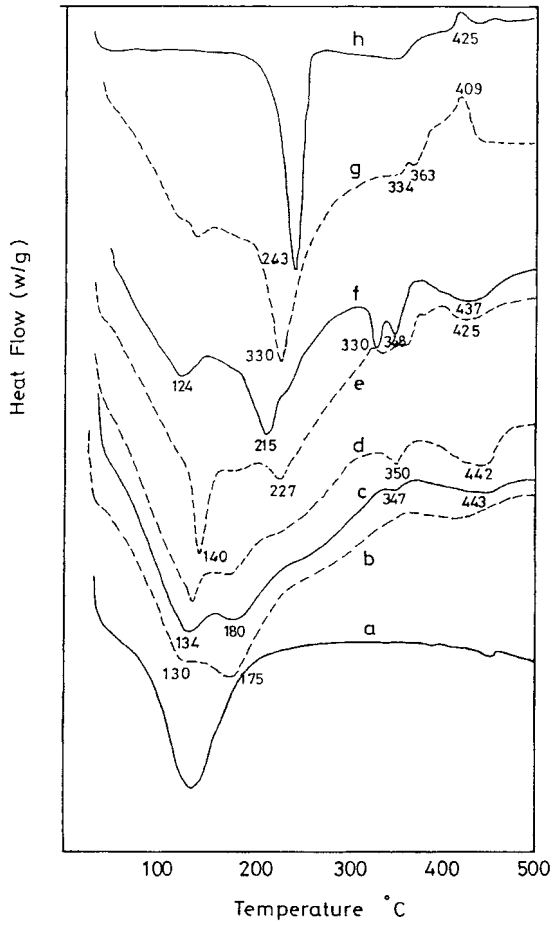

Figure 3. DSC curves of pure AP (a) and AMV supported on AP: 3% (b); 7% (c); 10% (d); 15% (e); 20% (f); 30% (g); and pure AMV (h).

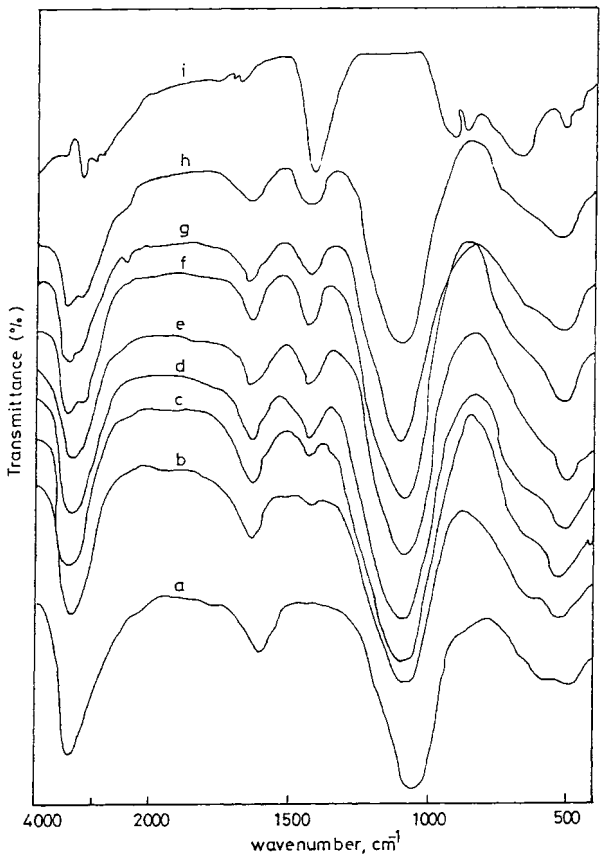

Figure 4. IR spectra of original samples of pure AP (a) and AMV supported on AP: 3% (b); 5% (c); 7% (d); 10% (e); 15% (f); 20% (g); 30% (h); and pure AMV (i).

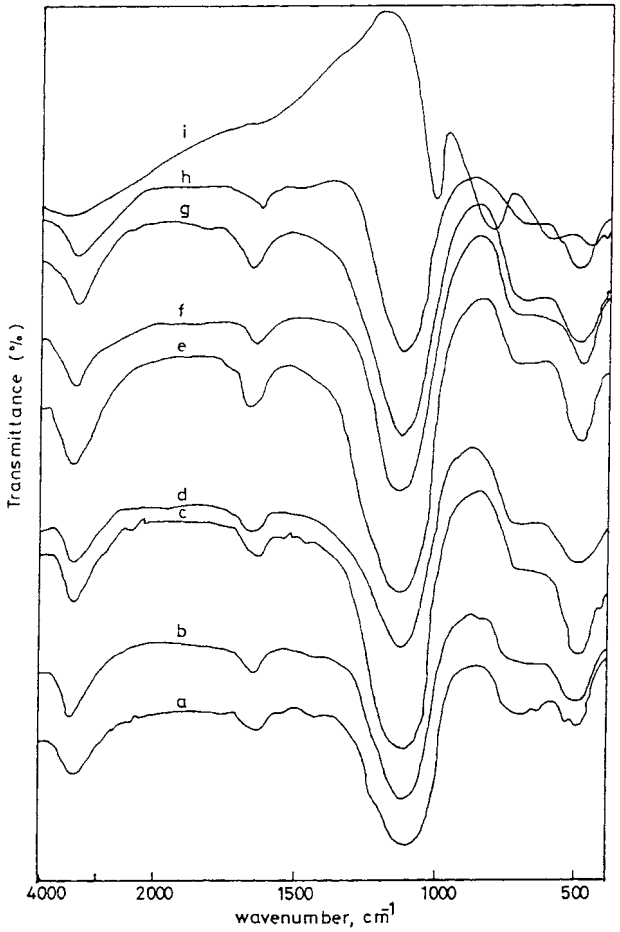

Figure 5. IR spectra of samples calcined at 400 °C for 4 h of pure AP (a) and AMV supported on AP: 3% (b); 5% (c); 7% (d); 10% (e); 15% (f); 20% (g); 30% (h); and pure AMV (i).

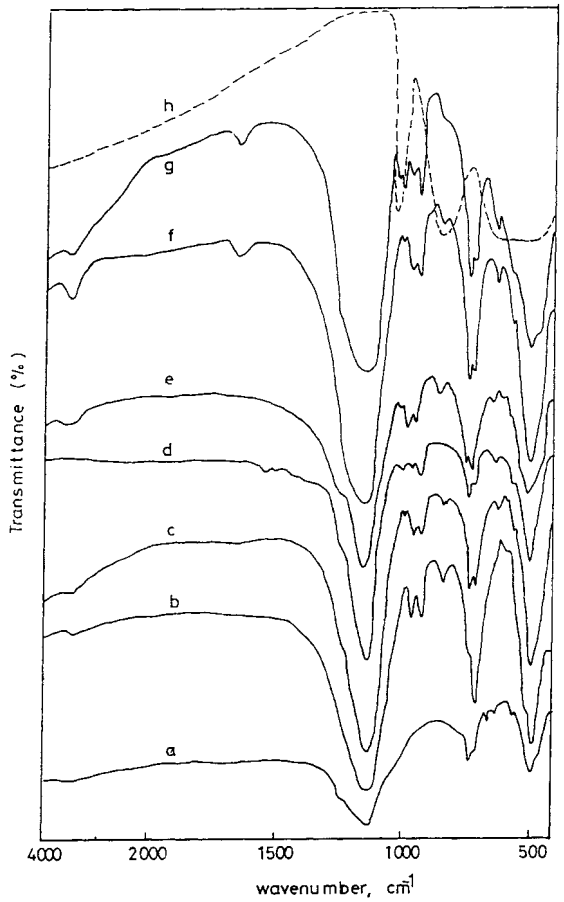

Figure 6. IR spectra of samples calcined at 600 °C for 4 h of pure AP (a) and AMV supported on AP: 3% (b); 7% (c); 10% (d); 15% (e); 20% (f); 30% (g); and pure AMV (h).

modes of the PO_4 tetrahedra, AlO_4 tetrahedra and AlO_4 (H_2O) octahedra.[17,18]

(ii) On addition of AMV up to 30 mol%, the same spectra were obtained except for a new broad band at about 1400 cm^{-1} due to the presence of AMV.[19]

(iii) Figure 5 shows the spectra of AMV supported on $AlPO_4$ calcined at 400 °C. It is clear that the spectra are similar to those of the original samples except that a decrease in the intensity of the band assigned at 3793 cm^{-1} is observed and new bands appear corresponding to the V_2O_5 (curve h). Moreover, V_2O_5 exhibited a band at 1020 cm^{-1} which is assignable to the V=O stretching vibration.[15] The band at 840 cm^{-1} was attributed to a combination band of V—O—V stretching and lattice vibrations.

Figure 6 shows the spectra of AMV supported on AP calcined at 600 °C. It shows that the bands due to the water molecules located in the interlayer space have disappeared. Moreover, new bands appeared at 960, 730, 710 and 620 cm^{-1} for the samples of $AlPO_4$ mixed with 3–30 mol% AMV. These new bands may be due to the formation of a new phase.

3.3 XRD investigation of the thermal products of AMV supported on $AlPO_4$

X-Ray diffraction patterns of AMV supported on AP calcined at 400 and 600 °C are represented graphically in Figs 7 and 8. Figure 7 shows that pure AP exhibits an amorphous structure. On addition of V_2O_5 up to 20 mol%, little crystallinity is observed in the amorphous nature of AP. Moreover, the line which is located at d (nm) = 33.8 may correspond to the formation of a β-$VOPO_4$ structure.[20] Furthermore, pure AP and mixed with AMV calcined at 600 °C exhibits a crystalline structure, as shown in Fig 8. It shows that the new phase, β-$VOPO_4$, developed and gave a predominant diffraction line located at d (nm) = 33.8 for the samples containing V_2O_5/AP at ratios < 20 mol%. In addition, interesting results are obtained on addition of 20 or 30 mol% V_2O_5 into AP, curves d and e. The new predominant line assigned at d (nm) = 41.1 corresponds to the formation of a new phase,[20] β''-$(VO)_2P_2O_7$. In addition to this new phase, the diffraction lines detected at d (nm) = 30.0 and d (nm) = 25.0 correspond to the existence of $AlVO_4$ and Al_2O_3 respectively.[15,21] However, XRD results allow the conclusion that the formation of crystalline structures of β-$VOPO_4$ and β'' -$(VO)_2P_2O_7$ depend on the content of V_2O_5 and on the calcination temperature.

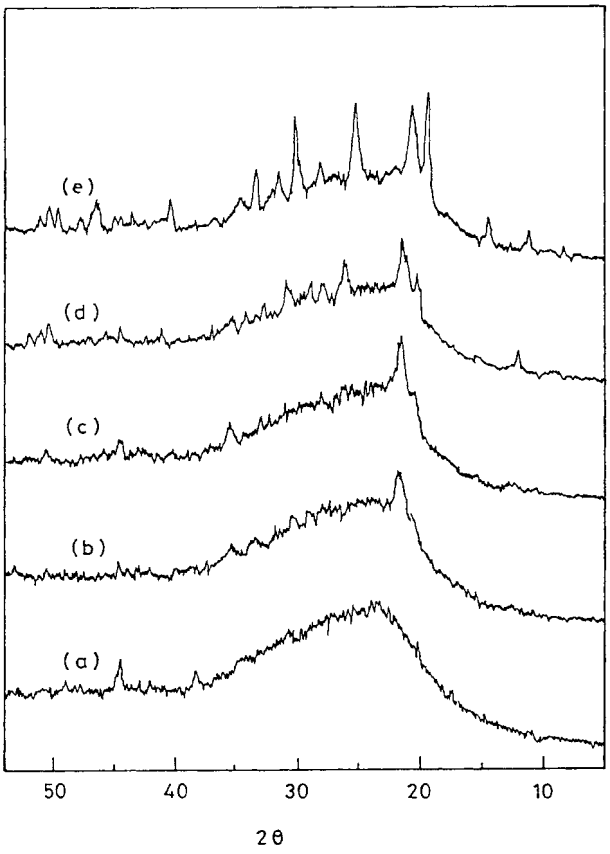

Figure 7. X-ray diffraction patterns of pure AP (a) and AMV supported on AP: 3% (b); 7% (c); 10% (d); and 20% (e) of the samples calcined at 400 °C.

3.4 Surface properties of pure and mixed catalysts

The adsorption isotherms of nitrogen were measured on pure AP and mixed with different ratios of AMV calcined at 400 and 600 °C. These isotherms lie between types I and II of the Brunauer classification[22] with closed hysteresis loops at intermediate relative pressure. The specific surface areas of all investigated catalysts, S_{BET}, in $m^2 g^{-1}$ are shown in Fig 9. It shows the variation of S_{BET} with the V_2O_5 content for the samples calcined at 400 and 600 °C, curves a and b respectively. These results indicate that:

(i) The samples calcined at 400 °C suffered a significant decrease in S_{BET} value by increasing the content of V_2O_5
(ii) For the samples calcined at 600 °C, the addition of 1–5 mol% V_2O_5 decreases the surface area of AP while it increases only a little on increasing the content of V_2O_5 up to 30 mol%.
(iii) A drastic reduction in the S_{BET} values of the materials calcined at 600 °C is obtained.

From the pore volume distribution curves and V_{a-t} plots, the following conclusions can be made:

(i) Pure $AlPO_4$ contains a mesopore structure.
(ii) The addition of V_2O_5 to AP produces new pores which have a larger pore radii. Moreover, the number of pores, as shown by the height of the distribution curve, is substantially reduced when

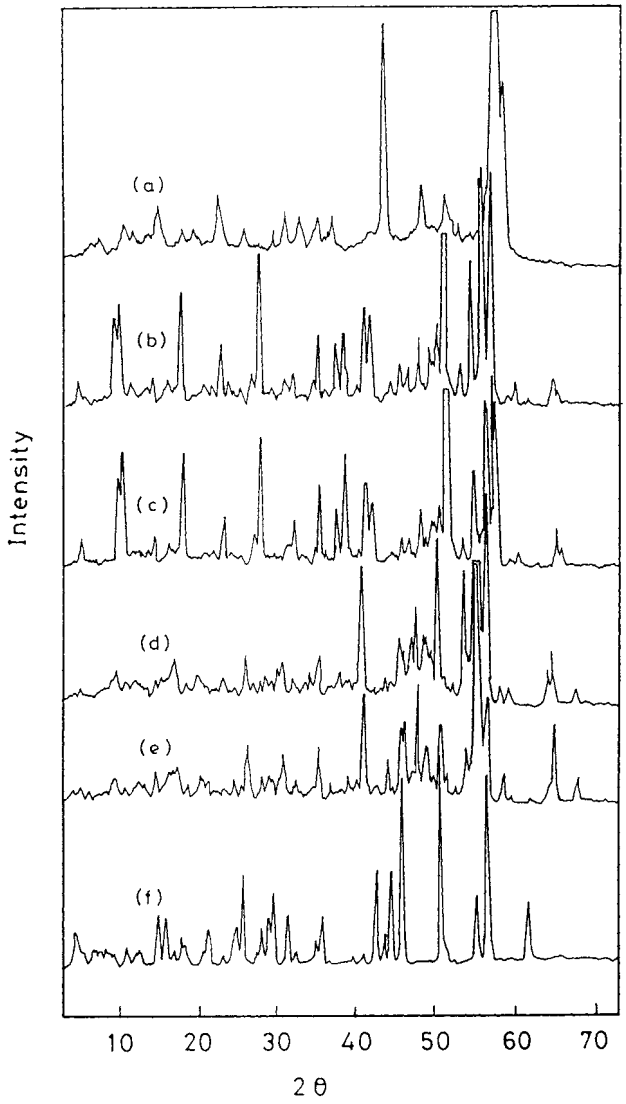

Figure 8. X-ray diffraction lines of samples calcined at 600 °C for 4 h of pure AP (a) and AMV supported on AP: 5% (b); 10% (c); 20% (d); 30% (e); and pure AMV (f).

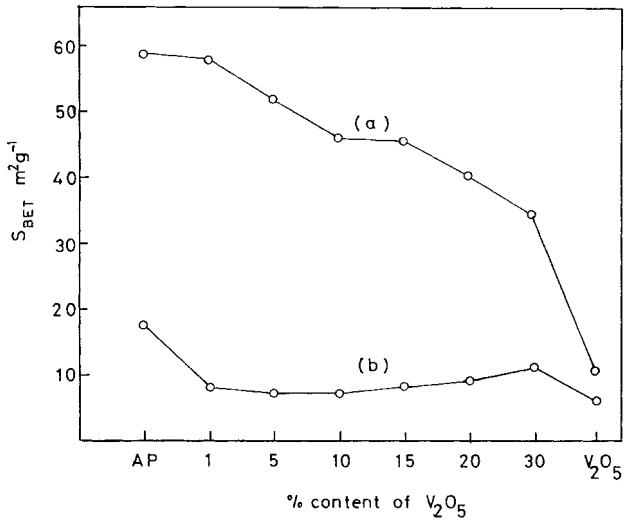

Figure 9. S_{BET} variation with amount of V_2O_5 supported on AP of the samples calcined at 400 °C (a) and at 600 °C (b).

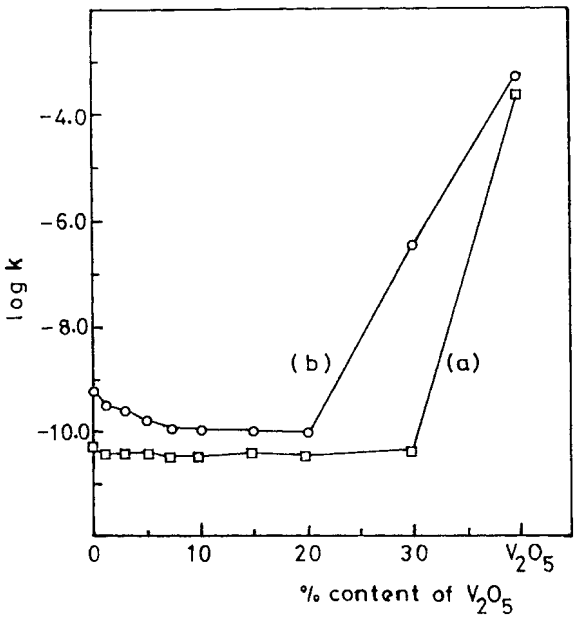

Figure 10. Variation of log σ with amount of V_2O_5 supported on AP of the samples calcined at 400 °C without (a) and with (b) alcohol.

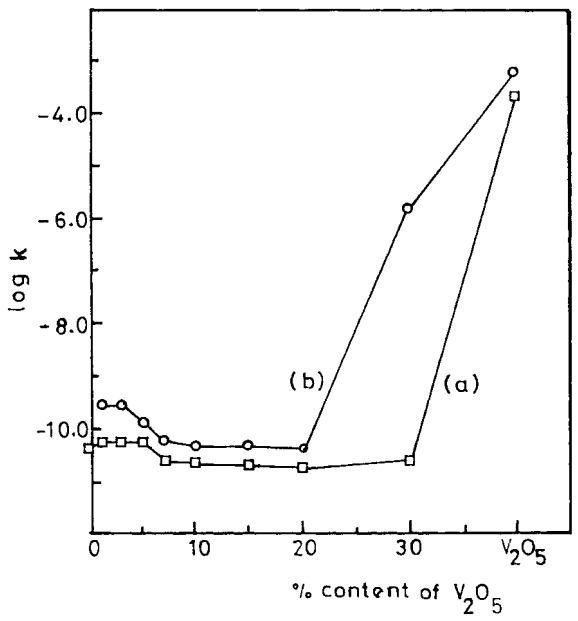

Figure 11. Variation of log σ with amount of V_2O_5 supported on AP of the samples calcined at 600 °C without (a) and with (b) alcohol.

the V_2O_5 ratio is increased up to 30 mol%. Consequently the reduction in the number of mesopores is responsible for the decrease in the surface areas of the supported catalysts calcined at 400 °C (curve a).

(iii) The texture of the solids calcined at 600 °C contains wide pores. These pores may be created by the sintering process which is responsible for a sharp decrease in S_{BET} values.

3.5 Electrical conductivity

The electrical conductivity measurements with and without ethanol vapor have been carried out at 210 °C on all catalysts calcined at 400 and 600 °C. The experimental conditions used are similar to those used in catalytic activity runs. Figures 10 and 11 show the variation of log k with the% content of V_2O_5. Curves a (Figs 10 and 11) show that without ethanol (air only), little variation is observed in the conductivity value of pure AP and mixed with V_2O_5 up to 30 mol%. This behavior may be attributed to the small change in charge carriers. According to XRD patterns (Fig 8), it can be suggested that the formation of β-$VOPO_4$ which contains V ions in the V^{5+} valence state should decrease the V^{4+}/V^{5+} ratio and consequently should decrease the electron jumping on the catalyst surface. On the other hand, curves b (Figs 10 and 11) show that the addition of alcohol gives a similar trend to that obtained in the case of air only for the samples containing V_2O_5 up to 20 mol%. Moreover, a remarkable increase in the conductivity of the catalyst containing 30 mol% V_2O_5 is obtained. This increase in the conductivity may be attributed to the presence of permanent electrochemical equilibrium[23] can be assumed.

$$V^{5+} \leftrightarrow V^{4+} + P^+$$

Since vanadium ions are involved also in vanadyl ions can be written as:

$$(V^{V}O)^{3+} \leftrightarrow (V^{IV}O)^{2+} + P^+$$

From the above equations, a positive hole P^+ (or position), corresponds to an electron vacancy in the valency band of O^{2-} anions. Such holes can be filled by an electron jumping from a neighboring anion according to the following equation:

$$O^{2-} + P^+ \rightarrow O^-$$

O^- anions correspond to the chemical site of a hole. The creation of holes should enhance the electron exchange between the alcohol and catalyst surface while the consumption of holes during the reactions leads to the decrease of the catalyst's conductivity. In agreement with this suggestion, we observed that when the alcohol is admitted onto the catalyst surface, the conductivity increases up to maximum followed by a continuous decrease until a constant value is reached after 1 h for all samples containing V_2O_5 up to 30 mol%.

The width of the energy gap is important in controlling the number of molecules which can be chemisorbed in the course of a catalytic reaction and the nature of the chemical bond between the molecule and the surface. These factors control at the same time the activity and the mechanism of the catalytic reaction. Accordingly, the influence of the catalytic reaction temperature on the electrical conductivity value with and without ethanol was studied in the range 150–320 °C. The results indicated that the

Table 1. Activation energy in kJ of V_2O_5 supported on $AlPO_4$ calcined at 400°C for 4h

	mol% AMV				
	0	1	5	20	30
E_a (air only)	34.6	22.6	21.2	20.8	21.7
E_a (alcohol + air)	20.8	20.8	18.4	13.8	13.8

electronic exchange, ie the electrical conductivity value, increases on increasing the reaction temperature. Plots of log k against $1/T$ of pure AP and mixed with V_2O_5 can be fitted to an Arrhenius relationship.[24]

$$k = k_o \exp^{-E_a/RT}$$

where k is the electrical conductivity, k_o is the pre-exponential factor and E_a is the activation energy for migration of charge carriers. Values of E_a obtained by least squares fitting of the data are given in Table 1.

From Table 1 it can be easily seen that in absence of alcohol the activation energy of AP sharply decreases on addition of 1 mol% V_2O_5, while a small decrease is obtained on increasing the V_2O_5 content up to 30 mol%. On the other hand, on the admission of ethanol + air a further decrease in the activation energies is observed. This behavior is probably due to the pinning of the Fermi potential. The decrease in the activation energy should enhance and facilitate the chemisorption of ethanol and consequently the chemical reaction on the catalyst surfaces.

3.6 Catalytic activity measurements

The catalytic decomposition of ethanol was carried out over the catalysts calcined at 400 and 600°C for 4h. The measurements of the conversion and selectivity (in %) were made after 2h to achieve steady - state conditions. The reaction conditions were: 0.5g catalyst weight, 150 cm^3 min^{-1} total flow rate, 1.6% alcohol feed and 210°C reaction temperature. The analysis of the gas mixture after reaction revealed that ethene and diethyl ether were the only products. The experimental results for the catalysts calcined at 400°C are represented in Fig 12 which shows that pure AP possesses low activity and low selectivity towards ethene formation whereas it is selective towards diethyl ether formation.

On the other hand, the addition of V_2O_5 up to 10 mol% led to an increase in both conversion and selectivity towards ethene formation, while selectivity for diethyl ether formation sharply decreased. Further increase in the content of V_2O_5 up to 30 mol% shows a steady increase in both activity and selectivity towards ethene formation. However the product profiles for ethanol dehydration show that both diethyl ether and ethene are present from the onset of the reactions, indicating that both reaction products are formed by direct dehydration, ie they are primary reaction products coming from ethanol through a parallel reaction net work. A primary product is defined as

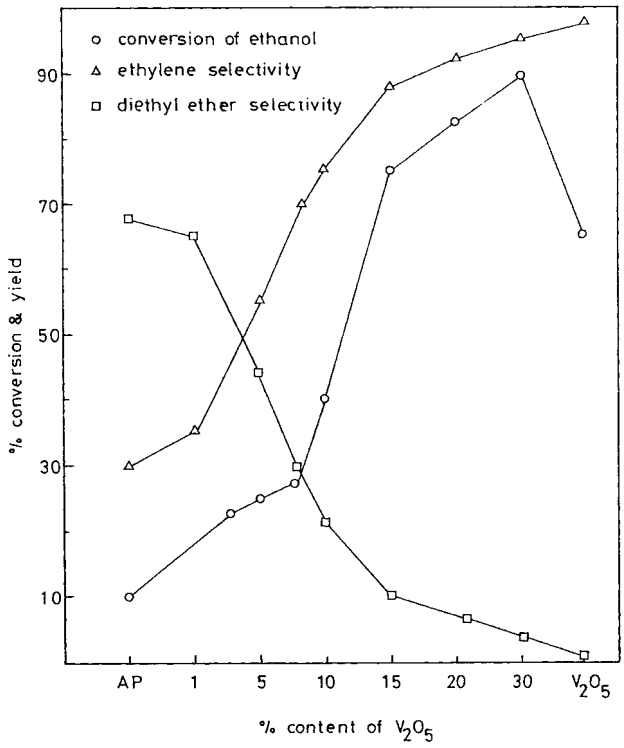

Figure 12. Variation of ethanol conversion and yields of ethylene and diethyl ether with amount of V_2O_5 supported on AP of the samples calcined at 400°C.

that which is produced from the reactant no matter how many surface intermediates may be involved in its formation. However, diethyl ether is an unstable product since a sharp decrease in its selectivity is observed due to the fact it also participates in the formation of ethene. So ethene is a primary plus a secondary stable reaction product. A secondary product is formed from a primary product no matter how many surface intermediates may be involved in its formation. Thus, the pathway of the formation of diethyl ether and ethene from ethanol dehydration on $AlPO_4/V_2O_5$ systems is a combination pathway of parallel and consecutive reactions, as shown in Scheme 1.

According to the results obtained, it is clear that the addition of V_2O_5 to AP led to an effective change in the dehydration processes. It is known that the AP surface possesses acid sites capable of taking part in the catalytic reactions. This has been shown in several ways.[16,25] Thus, the catalytic activity of AP is affected by two factors, the chemical nature of the surface (number and strength of acid sites) and the texture of the solid. Also, it was found that transition metal

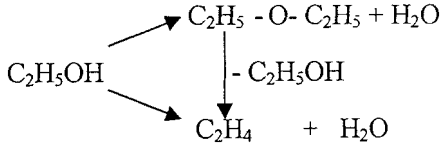

Scheme 1

substitution into certain aluminum phosphate catalysts enhanced acidity, as indicated by enhanced butane cracking activity.[26] Consequently, it appears that the addition of V_2O_5 (acid catalyst) may activate the acid sites present on the $AlPO_4$ surface and/or create new sites via the existence of a new phase resulting from the interaction between V_2O_5 and $AlPO_4$. However, a significant improvement of the catalytic performance is observed for the ethanol conversion and for the selectivity to ethene when the ratio of V_2O_5 increases up to 30 mol%. This effect can be correlated with changes in the microstructure of the vanadium phosphorus oxide catalysts as indicated by XRD and IR spectroscopy. The formation of β-$VOPO_4$ and β''-$(VO)_2P_2O_7$ phases during the activation of the precursor may change the V^{4+}/V^{5+} balance and consequently influence the catalytic performance. Moreover, the high selectivity towards the formation of ethene may be associated with catalysts with high V^{4+} contents. It is very tempting to suggest that this species is primarily responsible by interacting directly with adsorbed ethanol. However, in the literature, the vanadium ions in such catalysts have been shown to undergo redoxcycles ($V^{4+} \rightleftharpoons V^{5+}$) during the reaction.[27] Thus, our prepared catalysts initially contain β-$VOPO_4$ and β''-$(VO)_2P_2O_7$. Moreover, during the reaction β-$VOPO_4$ is slowly converted to vanadyl pyrophosphate in a reaction mixture in which the V ions are in the V^{4+} state. In addition, we can suggest that the formation of the above new phases accompanies the formation of Al_2O_3, as indicated by XRD. The Al_2O_3 may form some kind of solid solution with V_2O_5.[28] The ionic radii of Al^{3+} and V^{5+} ions are 5.0 and 5.9 nm, respectively.[29] Therefore, some of the Al^{3+} ions could be dissolved in the V_2O_5 lattice through location in the interstial position and/or cationic vacancies, according to the following doping mechanism using Kröger's notations.[30]

$$Al_2O_3 + 3V^{5+} \rightarrow 2Al\boxed{\Delta} + 3V^{3+} + 3/2O_{2(g)}$$

$$Al_2O_3 + 6V^{5+} \rightarrow 2Al\boxed{\Delta} + 6V^{4+} + 3/2O_{2(g)}$$

$$Al_2O_3 + 2V^{3+} + O_{2(g)} \rightarrow 2Al(V^{5+}) + 2V^{5+}$$

Al $\boxed{\Delta}$ represents Al^{3+} located in an interstitial position or in a cationic vacancy, and $Al(V^{5+})$ denotes a trivalent aluminum ion located in the position of host V^{5+} cations present in the V_2O_5 lattice. Thus the formation of V^{4+} created by the above equations together with V^{5+} (present in the β-$VOPO_4$ spinel) are responsible for such an increase in the catalytic activity of the supported catalysts. Moreover, from the electrical conductivity results, it is important to mention that the observed higher degree of conversion of ethanol to ethene for the samples containing V_2O_5 ($\geq$ 10 mol%) may not result from the optimum ratio of V^{4+}/V^{5+} cations but could also be related to the value of the Fermi potential. Thus, the decrease in the activation energy of the $AlPO_4$ by the addition of V_2O_5 may facilitate the electron exchange between the alcohol and the catalyst surface.

It is worth mentioning that the catalytic decomposition of ethanol over the catalysts calcined at 600 °C was carried out (results not included in this paper). A drastic decrease in both conversion and selectivity of the catalysts was obtained. This result may be attributed to the formation of crystalline β-$VOPO_4$ and β''-$(VO)_2P_2O_7$ phases which exhibit low surface area values due to the sintering process, as indicated in Fig 9.

4 CONCLUSIONS

The main conclusions that can be derived from the results obtained are:

(1) Various ratios of V_2O_5 supported on $AlPO_4$, prepared by an impregnation method and preheated at 400 °C, act as active and selective catalysts for ethanol conversion reactions.
(2) The formation of crystalline β-$VOPO_4$ and β''-$(VO)_2P_2O_7$ spinels produces desirable catalysts for enhancing the dehydration process of ethanol towards ethene formation.
(3) The higher degree of conversion of ethanol to ethene for the samples containing V_2O_5 ($\geq$ 10 mol%) may not only be due to the optimum ratio of V^{4+}/V^{5+} but also due to the value of the activation energy of charge carriers.
(4) A drastic reduction in the catalytic activity and selectivity of all prepared samples preheated at 600 °C is observed.

REFERENCES

1 Bozik JE, Vogel RF, Kissin YV and Beach DL, Metallophosphate-supported Zeigler-natta catalysts for ethylene polymerization. *J Appl Polym Sci.*, **29**:3491–3497 (1984).
2 McDaniel MB, *Advances in Catalysis* Vol 33, Academic Press, New York. p 47 (1986).
3 Marcelin G, Vogel RF and Swift HE, Alumina–aluminum phosphate as a large-pore support and its application to liquid phase hydrogenation. *J Catal* **83**:42–49 (1983).
4 Bautista FM, Compela JM, Garcia A, Luna D, Marinas JM, Romero AA, Colon G, Navio JA and Macias M, Structure, texture, surface acidity and catalytic activity of $AlPO_4$–ZrO_2 (5–50 wt% ZrO_2) catalysts prepared by a sol–gel procedure. *J Catal* **179**:483–494 (1998).
5 Hucknall DJ, *Selective Oxidation of Hydrocarbons*, Academic Press, London (1974).
6 Gellings PJ, *Catalysis*, Vol 7, Royal Society of Chemistry, London. p 105 (1985).
7 Bond GC and Flamerz S, Structure and reactivity of titania-supported oxide, IV. Characterization of dried vanadia/titania catalysts. *Appl Catal* **46**:89–102 (1989).
8 Reddy BM, Narsimha K, Rao PK and Mastikhin VM, Influence of MoO_3 and WO_3 on the dispersion and activity of V_2O_5 in vanadia–silica catalysts. *J Catal* **118**:22–30 (1989).
9 *Catal Today* **16**:1–8 (1993), Proceedings, Vanadyl Pyrophosphate Catalysts (Centi , G. Ed).
10 Guliants VV, Benziger JB, Sundaresan S, Yao N and Wachs IE, Evolution of the active surface of the vanadyl pyrophosphate catalysts. *Catal Lett* **32**:379–386 (1995).
11 Sananes MT, Hutchings GJ and Volta JC, On the role of the

$VO(H_2PO_4)_2$ precursor for *n*-butane oxidation into maleic anhydride. *J Catal* **154**:253–260 (1995).
12 R'Kha C, Vandeborre MT and Livage J, Spectroscopic study of colloidal $VOPO_4.2H_2O$. *J Solid State Chem* **63**:202–215 (1986).
13 Smith JV (Ed), *X-Ray Powder Data File*, American Soc for Testing Materials, Philadelphia (1960).
14 Said AA, Hassan EA and Abd El-Salaam KM, Electrical conductivity and thermogravimetric studies of the thermal decomposition of cobalt carbonate. *Surf Technol* **20**:123–130 (1983).
15 Said AA, Influence of Al_2O_3 support on the thermal decomposition of ammonium metavanadate. *J Mat Sci* **27**:5869–5872 (1992).
16 Campelo JM, Gracia A, Herencia JF, Luna D, Marinas JM and Romero AA, Conversion of alcohols (α-methylated series) on $AlPO_4$ catalysts. *J Catal* **151**:307–314 (1995).
17 Davis ME, Monte C, Hathaway PE, Arhancet JP, Hasha DL and Garces JM, Physicochemical properties of VPI-5. *J Am Chem Soc* **111**:3919–3924 (1989).
18 Pluth JJ and Smith JV, Hydrate of aluminum phosphate ($AlPO_4.1.5H_2O$) with PO_4, AlO_4 and AlO_4 $(H_2O)_2$ groups and encapsulated water. *Acta Crystallog Sect C Cryst Struct Commun* **9**:1118–1120 (1986).
19 Frederickson LD and Hausen DM, Infrared spectra–structure correlation study of V—O compounds. *Anal Chem* **35**:818–827 (163).
20 Ben Abdelouahab F, Olier R, Guilhaume N, Lefebvre F and Volta JC, A study by *in situ* laser raman spectroscopy of VPO catalysts for a-butane oxidation to maleic anhydride. *J Catal* **134**:151–167 (1992).
21 Yamaguchi O, Formation of AlVO4 (aluminum vanadate) solid solution from alkoxide. *J Am Ceram Soc* **70**:198–200 (1987).
22 Brunauer S, Deming LS, Deming WS and Teller E, A theory of the Van der Waals adsorption of gases. *J Am Chem Soc* **62**:1723–1732 (1940).
23 Herrmann JM, Vernoux P, Bere KE and Abon M, *In situ* study of redox and of p-type semiconducting properties of vanadyl pyrophosphate and of V–P.O catalysts during the partial oxidation of *n*-butane to maleic anhydride. *J Catal* **167**:106–117 (1997).
24 Morrison SR, In *Chemical Physics of Surfaces*, Plenum, New York. p 70 (1977).
25 Campel JM, Garcia A, Gutierrez JM, Luna D and Marinas JM, Skeltal isomerization of cyclohexene on $AlPO_4$ catalysts. *Can J* **61**:2567–2571 (1983).
26 Flanigen EM, Patton RL and Wilson ST, Structural, synthetic and physicochemical concepts in aluminophosphate-based molecular sieves. *Stud Surf Sci Catal* **37**:13–27 (1988).
27 Hodnett BK, Vanadium–Phosphorus oxide catalysts for the selective oxidation of C4 hydrocarbons to maleic anhydride. *Catal Rev Sci Eng* **37**:373–424 (1985).
28 Abdel-Wahab MMM and Said AA, Influence of the formation of aluminum spinel, AlVO4, on the catalytic activity of V2O5 support on γ-alumina. *Collect Czech Chem Commun* **59**:1983–1990 (1994).
29 Greenwood NN, *Ionic Crystals Lattice Defects and Non-Stoichiometry*, Butterworth, London. p 40 (1968).
30 Kröger FA. *Chemistry of Imperfect Crystals*, North Holland, Amsterdam (1964).